Impact of Tooth Surface Pitting and Friction on Load Transfer and Static Transmission Error in Spur Gears

Iqbal Shareef*
Department of IMET
Bradley University)
Peoria, IL 61625 USA
Shareef@bradley.edu
*Corresponding author

Timothy Krantz
Research and Engineering Directorate
NASA Glenn Research Center
Cleveland, OH 44135 USA
timothy.l.krantz@nasa.gov

Wasiq A.M Abdul
Department of IMET
Bradley University)
Peoria, IL 61625 USA
mohammad202026@outlook.com

***Abstract*— This study investigates the combined influence of tooth surface pitting and friction on the static performance characteristics of involute spur gear pairs. A numerical framework based on linear elastic static analysis is employed to evaluate gear meshing behavior for both undamaged and damaged teeth. Localized surface damage is represented using parabolic pit profiles introduced at multiple locations along the line of action, with three pit depths considered to simulate increasing damage severity. In addition, the coefficient of friction varies from zero to 0.30 in increments of 0.05 to examine frictional effects under a wide range of operating conditions.**

The combined effects of surface damage and friction are quantified through key static performance metrics, including static transmission error (STE), tooth load distribution, tooth root stress, contact stress, gear moment, and bearing force. Results indicate that STE variation increases monotonically with both pit depth and coefficient of friction, with the most pronounced effects occurring when damage is located near the pitch point. Surface pitting causes localized reductions in tooth load and contact stress, while adjacent teeth compensate to maintain torque equilibrium. Friction further amplifies variations in STE, root stress, gear moment, and bearing force. The findings highlight the strong coupling between surface damage geometry and frictional effects, underscoring the importance of accounting for both factors when assessing the performance of spur gear transmissions.

Keywords* — *Static Transmission Error, Tooth Surface Pitting, Coefficient of Friction, Spur Gear Damage, Friction Effects, Tooth Load Distribution, Gear Performance

I. Introduction

Gears are fundamental components for power transmission in industrial machinery, automotive systems, aerospace applications, and robotics. Elastic tooth deflection, manufacturing deviations, and geometric imperfections contribute significantly to transmission irregularities in geared systems. Bonori and Pellicano [1] demonstrated that tooth deflection and non-smooth contact behavior introduce transmission error, which acts as a primary excitation source for vibration and noise. Chaari et al. [2] further showed that poor operating conditions, including manufacturing errors, inadequate lubrication, and tooth faults, markedly increase dynamic excitation in gear transmissions.

Among excitation metrics, static transmission error (STE) is widely recognized as the dominant source of gear-induced vibration and noise under quasi-static conditions. Randall [4] established transmission error as a key indicator of gear mesh quality, and McFadden's work [5], [6] demonstrated that meshing vibration characteristics are directly linked to STE. Subsequent studies confirmed that low-frequency vibration components and noise are strongly correlated with STE, rather than purely dynamic effects [7–9]. Consequently, STE has become a central parameter for gear design and performance, fault sensitivity, and transmission smoothness.

During service, gear performance can deteriorate due to progressive surface and subsurface damage. Such damage may reduce transmission efficiency and can progress to cause failure. Tooth surface pitting is one of the most prevalent forms of gear damage, typically initiated by repeated contact stresses and elastic deformation under load [3]. Pitting alters local contact conditions and mesh stiffness, redistributing load along the line of action and directly affecting STE—especially when damage occurs near the pitch point [8], [13], [14].

Early fault detection research focused on identifying changes in vibration signals caused by transmission irregularities. Randall [4] proposed vibration-based methods to detect and localize developing gear faults by analyzing frequency spectra measured externally on operating gearboxes. McFadden [5] introduced time-domain averaging techniques to isolate meshing harmonics, effectively detecting early gear failure, and later showed that phase modulation of meshing vibration can locate fatigue cracks within a gear tooth [6]. Zakrajsek et al. [7] applied time- and frequency-domain averaging to detect tooth fracture, pitting, and heavy wear in high contact ratio gear meshes. Although these techniques rely on measured vibration responses, the excitation driving these signatures is fundamentally linked to variations in transmission error.

Numerical and simulation studies have further clarified how surface damage affects gear transmission. Choy et al. [8] simulated vibration responses of gear systems with surface pitting, wear, and partial tooth fracture, showing that localized damage produces characteristic changes in transmission behavior. Kuang and Lin [9] studied the effect of tooth wear on vibration spectra by incorporating load-sharing alternation, mesh stiffness variation, damping, and friction, showing that surface degradation modifies effective mesh stiffness and alters transmission error. Dempsey [10] demonstrated that oil debris accumulation can predict pitting progression in spur gears using fuzzy logic analysis.

The interplay between friction, surface damage, and transmission error has been explored through analytical and numerical modeling. Howard et al. [11] showed that frictional forces significantly influence meshing behavior and load transfer, especially in the presence of cracks. Decker [12] proposed improved tooth analysis-based crack detection techniques, noting limitations in robustness and early fault identification. Liu and Pines [13] developed analytical models including pitting, wear, and root cracks, revealing that basic gear design parameters strongly influence damage detection sensitivity through their effect on STE.

Localized surface damage directly affects transmission error. Endo and Randall [14] compared spalling and root cracks, demonstrating that different damage types produce distinct STE signatures. Chaari et al. [15] and Hbaieb et al. [16] extended these findings to planetary and helical gears, showing that pitting and profile errors introduce additional excitation through stiffness variation and load redistribution.

Recent studies focus on quantitative evaluation of STE due to pitting and friction. Thunuguntla et al. [17] demonstrated that pit depth and location significantly influence mesh stiffness and STE, with the strongest effects at the pitch point. Shareef et al. [18] showed that both pit depth and friction coefficient increase STE variation. Happi [19] experimentally confirmed on pitted spur gears that increasing damage severity measurably alters quasi-static transmission behavior.

Finite element–based tooth contact models enhance STE prediction accuracy. Czakó et al. [20] used three-dimensional FEA for helical gears, showing strong agreement with experimental results. Liu et al. [21] emphasized, in a review of micropitting studies of steel gears, that surface topography, lubrication, and friction modify contact stiffness and influence damage initiation and progression. Im et al. [22] further refined STE estimation using enhanced tooth contact analysis incorporating measured profile errors.

Building on these foundations, recent works have leveraged static transmission error (STE) based analysis for design optimization, fault diagnostics under complex damage modes, and lubrication- and measurement-aware modeling. Abruzzo et al. [23] designed profile modifications using a design-for-manufacturing strategy explicitly guided by STE, demonstrating that STE-targeted modifications can improve dynamic behavior while remaining practical for production. Mark et al. [24] analyzed the frequency-domain behavior of transmission error in failing gears, showing how TE spectral features evolve with damage and providing a robust basis for condition monitoring in the presence of progressive faults. Ouyang et al. [25] performed comprehensive diagnosis of spur gears with pitting–crack coupling faults, highlighting interaction effects between surface and subsurface damage on vibration signatures and clarifying the diagnostic value of TE-related features under coupled degradation.

Zhao et al. [26] investigated the effect of tooth surface pitting under mixed lubrication, showing that lubricant regime alters dynamic characteristics and modulates the stiffness loss induced by pitting, thereby influencing STE and its harmonics. Extending beyond involute gearsets, Xu et al. [27] examined precision planetary cycloidal reducers and found that pin-tooth wear produces measurable changes in transmission error, underscoring STE's generality as a health indicator across gear classes and architectures. In crack-focused studies, Ren et al. [28] characterized the dynamic response of spur gear transmissions with crack faults, linking crack growth to changes in mesh stiffness variability and TE-driven excitations. Complementing diagnostics with prognostics, Liang et al. [29] proposed a model-based assessment of pitting propagation, relating damage progression to evolving STE and offering a path toward physics-informed life prediction. From a measurement perspective, Ji et al. [30] developed a quasi-static transmission error measurement approach based on an acceleration method, enabling practical TE acquisition that supports both model validation and in situ condition assessment.

II. Gear Design Parameters and Tooth Damage

A. *Gear Set and Design Parameters*

The spur gear pair examined in this study is summarized in Table I and illustrated in Fig. 1. The gear pair is an involute spur configuration with geometry and material properties chosen to be representative of aerospace-quality gears under accelerated contact-fatigue testing.

TABLE I. GEAR DESIGN PARAMETERS

Parameter	Value / Units
Number of teeth (z)	28
Pitch diameter (d)	88.9 mm
Outer diameter (d_a)	95.0 mm
Root diameter (d_f)	79.8 mm
Cicular pitch (p)	9.975 mm
Module (m)	3.175 mm
Pressure angle (α)	20°
Tooth thickness (at reference circle)	4.85 mm
Face width (b)	25.4 mm
Inner diameter (bore)	25.4 mm
Hob tip radius	1.02 mm
Young's modulus (E)	207 GPa
Poisson's ratio (ν)	0.30
Input torque	621.4 N·m

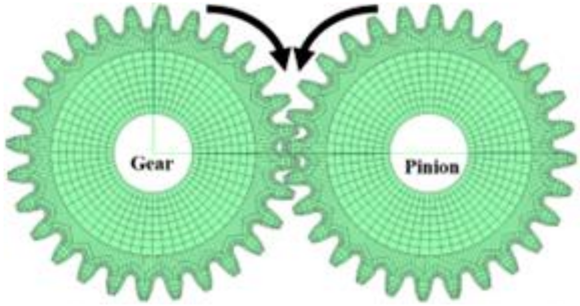

Fig. 1. Spur Gear Pair.

B. *Modeling Assumptions and Boundary Conditions*

Both the gear and pinion inner diameters are modeled as rigid circles. Their lateral degrees of freedom are coupled to ground through a bearing stiffness matrix with 876 kN/mm on the diagonal, representing high but finite lateral support compliance. The gear (wheel) inner diameter is constrained against rotation, while a constant input torque of 621.4 N·m is applied to the pinion inner diameter. Material behavior is linear elastic, and fillet root stresses are evaluated under a plane-stress assumption. All simulations are quasi-static and solved as a sequence of time-steps that advance the mesh position according to kinematics. The time increment is normalized such that 1.00 s corresponds to one tooth-pitch rotation of the pinion. A time-step of 0.05 s is used. The model is a combined finite element and surface integral approach. The contact solution is by the surface integral approach, while overall elastic deformation is by finite element method. The solution method makes sure that the surface integral and finite element deformations match at an appropriate boundary that is close enough to but not coincident with the gear teeth contacting points [31]. With such an approach there is no need to change the finite element mesh when pits are introduced to the analysis model.

The computational model has been applied to the analysis of multiple gearbox behaviors for the case of undamaged gears, and simulation results have been substantiated by experimental data [31-37]. Experimental validation was conducted at NASA Glenn Research Center as part of a collaborative test program involving NASA and the U.S. Army, in which strain gages were applied to the sun gear and ring gear of a helicopter planetary gearbox to measure tooth root strains in critical fillet regions. Additional details regarding the experimental configuration, numerical modeling approach, and simulation–experiment comparison is provided in Appendix A.

C. *Tooth Damage: Type and Realistic Geometries*

This study focuses on tooth surface pitting, a prevalent damage mode that perturbs local contact geometry and reduces mesh stiffness, thereby influencing quasi-static static transmission error (STE), load sharing, and stress distributions. Figure 2 presents typical pitting of flanks of spur gear teeth resulting from contact fatigue testing.

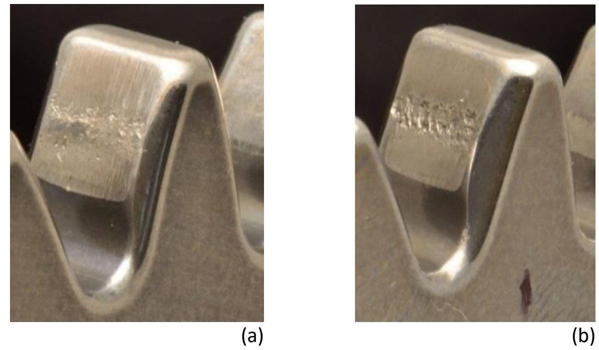

Fig. 2. Typical pitting for (a) mild and (b) moderate severities of damage.

To ground the modeling in realistic geometry, Fig. 3 shows a pit profile (red) as measured using a stylus profilometer and its parabolic approximation (blue), derived from NASA Glenn Research Center testing. The pit width is 0.4064 mm (0.016 in) and the depth is 0.0127 mm (0.0005 in)

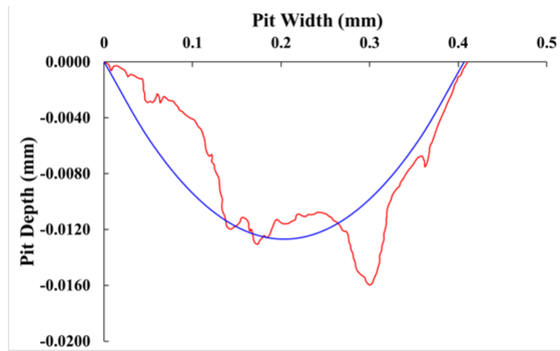

Fig. . 3. Geometric model of a gear tooth pit.

D. *Damage Parameterization and Locations*

In the simulations, pits are applied to tooth #1 of the pinion (driving gear). Seven pit locations are defined along the line of action with equal spacing between centers: one located at the pitch point, three toward the addendum side, and three toward the dedendum side. The pit width is maintained constant at 0.4064 mm, while the depth is varied from 0.0000 mm (no damage) to 0.1270 mm (0.005 in).

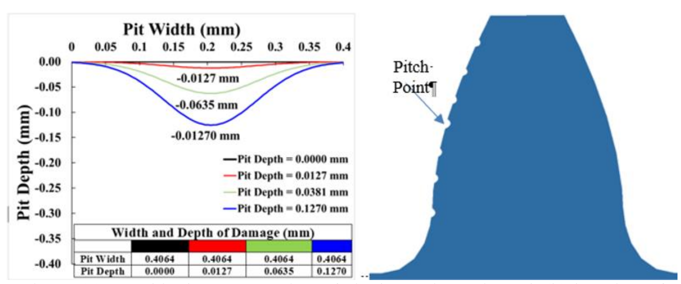

Fig. 4. (a) Graphical representation of pit shapes investigated. (b) location of pits of tooth surface

E. *Friction Modeling and Operating Range*

Because lubrication quality strongly influences wear and pitting progression, this study examines the influence of friction on quasi-static performance in both undamaged and pitted states. The coefficient of friction μ is varied from 0.00 to 0.30 in increments of 0.06.

III. Results

This section presents the numerical and qualitative results obtained from the finite element analysis of a spur gear pair with surface pitting damage. Static transmission error (STE), tooth loads, stress measures, gear moment, and bearing forces are evaluated for four pit depths and six coefficients of friction. A typical analysis required order of 3 to 5 minutes on a personal computer of modest specification with a 2.9 GHz processor and 8 GB of RAM. The results are presented without interpretation; discussion of underlying mechanisms is reserved for Section IV.

A. Static Transmission Error

The variation of static transmission error (STE) over five tooth pitches and two tooth pitches for different pit depths and coefficients of friction is shown in Fig. 5. The pitch point corresponds to time zero in the plots. For the undamaged case, STE variation remains relatively smooth over the entire mesh cycle. In contrast, the presence of surface pits introduces localized increases in STE magnitude.

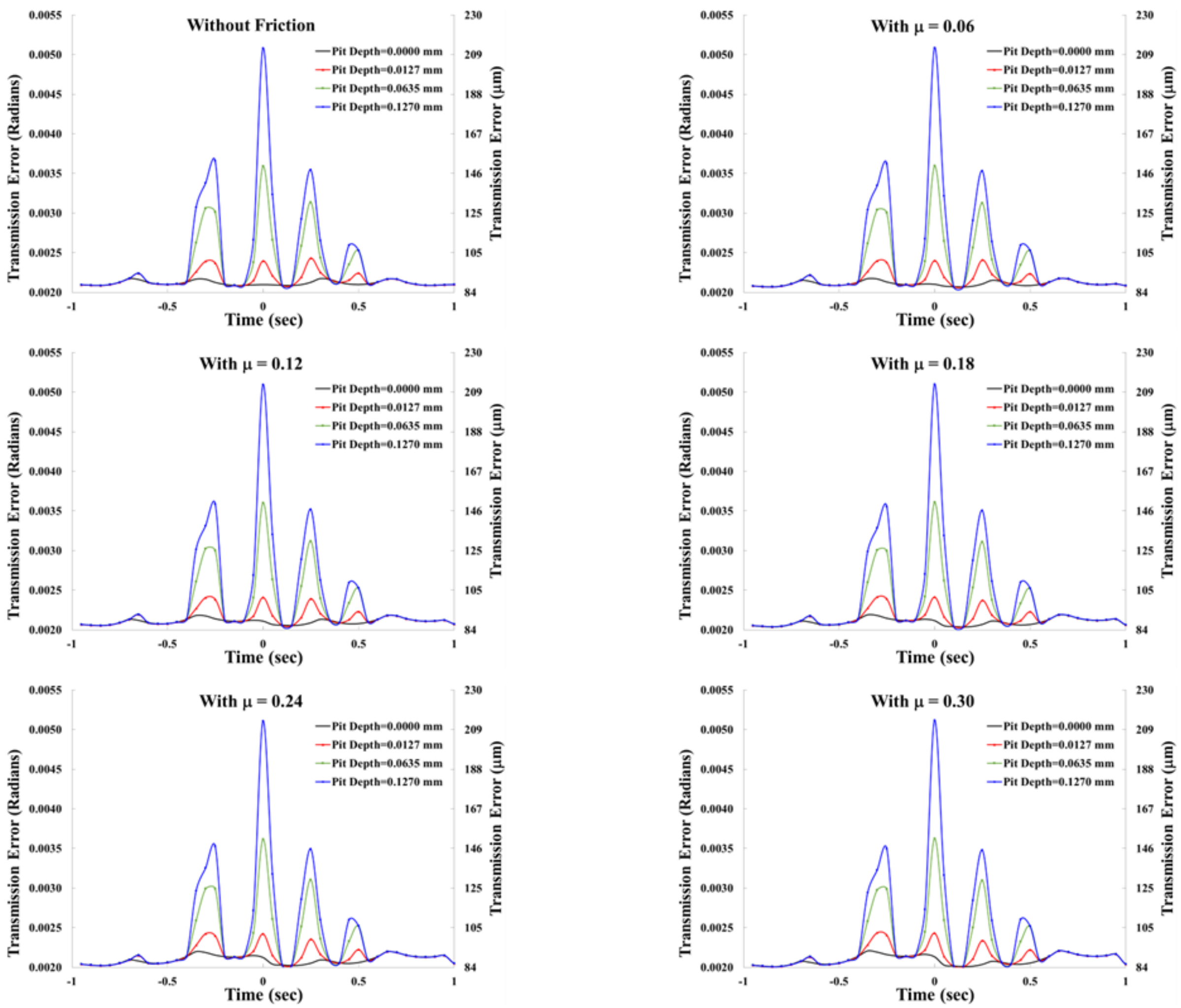

Fig. 5. Transmission error variations at different pit shapes and friction coefficients.

As pit depth increases, the amplitude of STE variation increases for all friction conditions. Among the seven modeled pit locations, excitation is observed primarily at five locations, indicating that pits located far toward the addendum and dedendum extremes do not come into contact with the mating tooth. Consequently, those pits do not contribute to STE variation. Damage located at the pitch point produces the most significant increase in transmission error compared to pits located away from the pitch.

The influence of friction on STE depends on pit location. At the pitch point, increased friction produces a slight increase in STE excitation, whereas for pits located on either side of the pitch point, higher friction results in a reduction of STE variation.

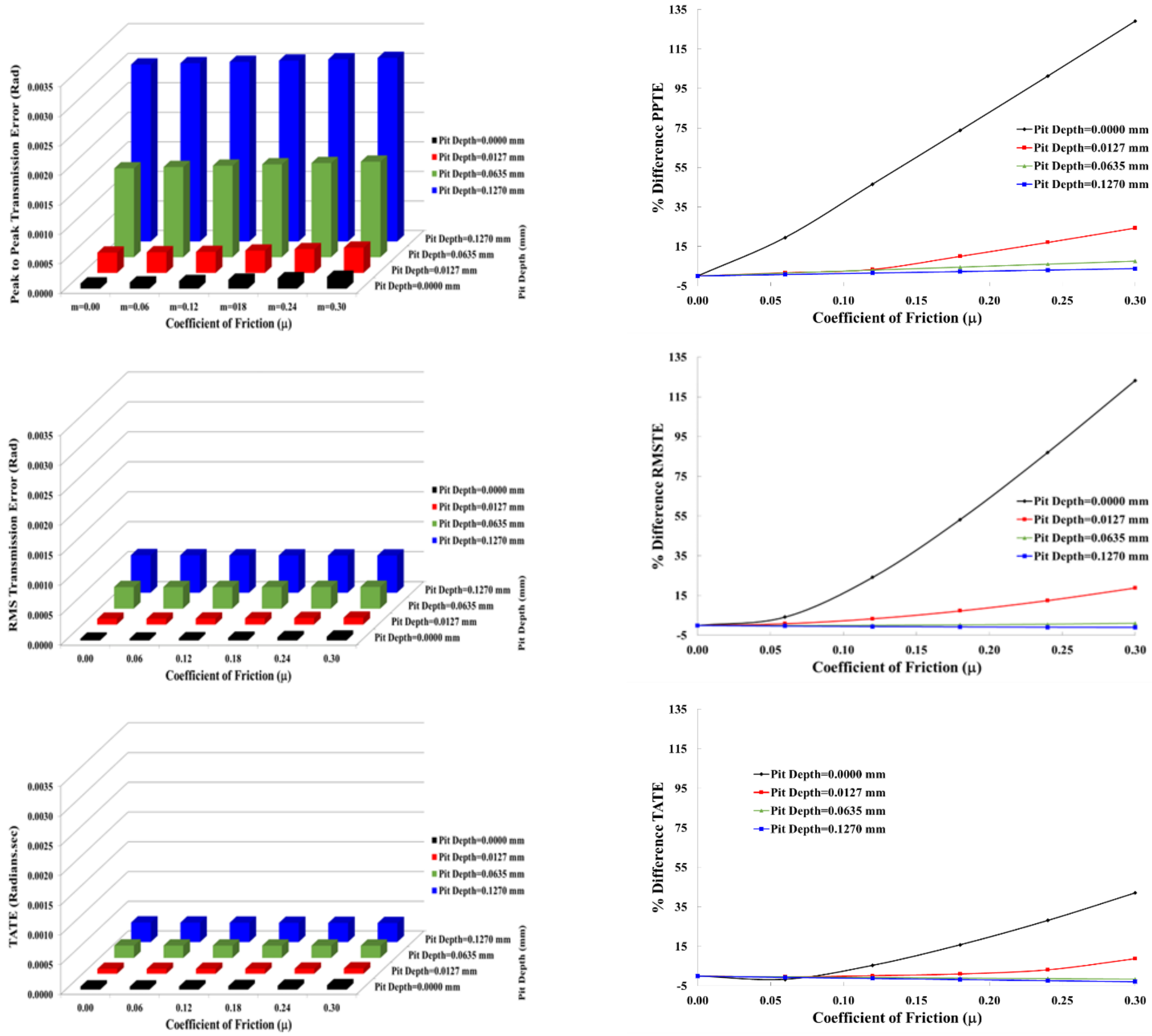

Fig. 6. Comparison of STE with three different metrics at different coefficient of frictions.

B. *Quantified STE Metrics*

Figure 6 compares STE quantified using three metrics: peak-to-peak transmission error (PPTE), root-mean-square transmission error (RMSTE), and total area transmission error (TATE). These three metrics were also used in [18]. In this work the metrics are calculated over two tooth pitch rotations to capture the influence of pits distributed from the root to the tooth tip.

PPTE increases with both increasing pit depth and increasing coefficient of friction. In contrast, RMSTE and TATE decrease with increasing friction for larger pit depths, while for the undamaged and shallow pit cases, RMSTE and TATE increase with friction. Across all friction conditions, increasing pit depth results in greater STE variation for all three metrics. The relative changes in STE metrics remain below 4% for the highest pit depths.

C. *Tooth Load Distribution*

The variation of load acting on Tooth 1 for different pit locations and coefficients of friction is shown in Fig. 7. In the absence of friction, pits cause localized reductions in tooth load due to partial or complete loss of contact. The pit located at the pitch point maintains the highest load and does not result in contact loss.

Loss of contact is more pronounced for pits located on the dedendum side than for those on the addendum side. Pits located farthest from the pitch point on both sides produce negligible changes in tooth load, consistent with the STE results. For the maximum pit depth, complete loss of contact causes the tooth load to drop to zero for a portion of the mesh cycle, regardless of friction level. Shallower pits produce correspondingly smaller load reductions.

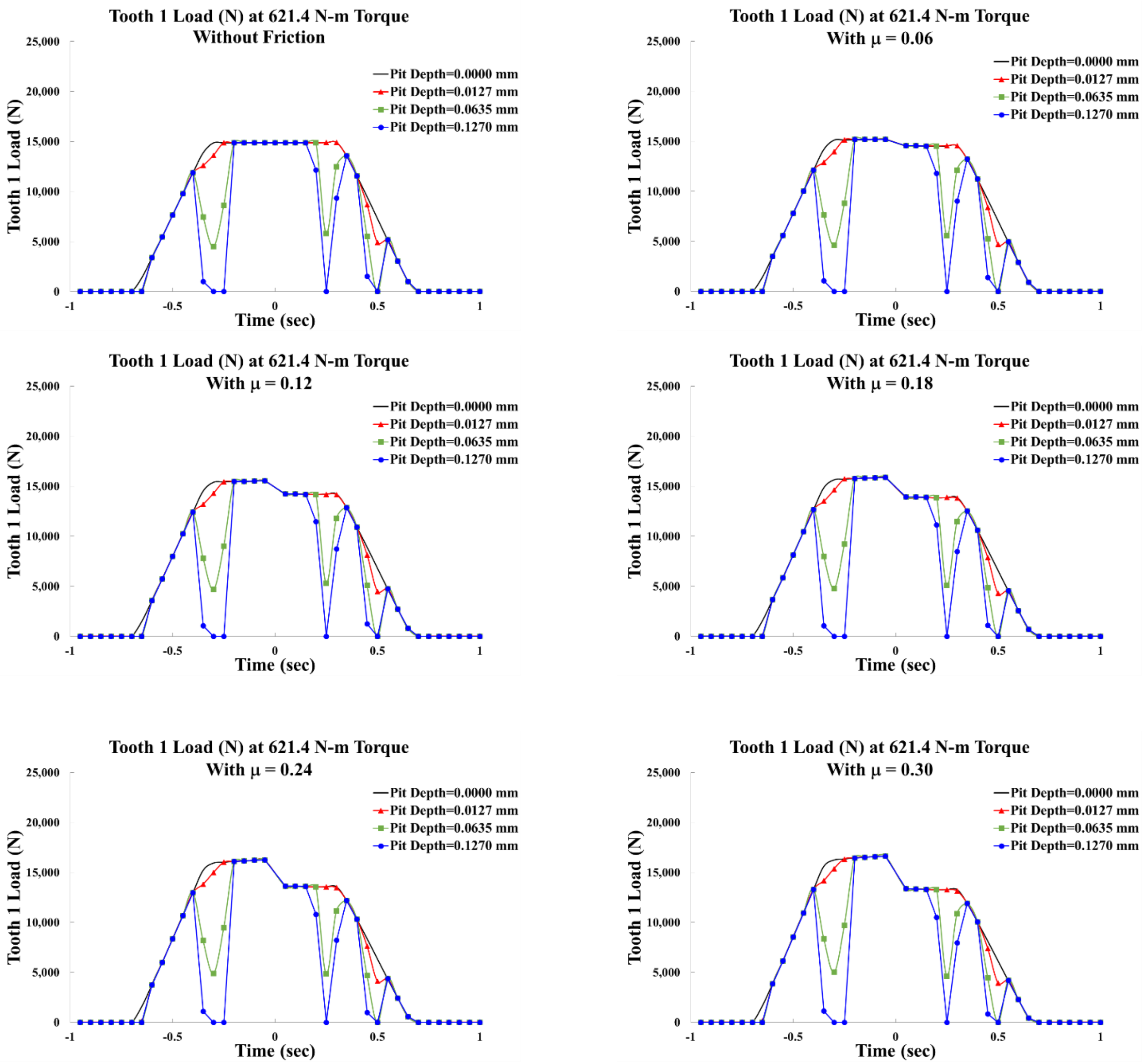

Fig. 7. Tooth number 1 load variations at different pits and friction.

As friction increases, the load distribution shifts: load increases on the dedendum side and decreases on the addendum side, with a gradual reduction at the pitch region.

D. Load Redistribution Among Adjacent Teeth

The redistribution of tooth load to adjacent teeth is shown for Tooth 28 and Tooth 2 in Figs. 8 and 9, respectively. When load on Tooth 1 is reduced due to pitting damage, the adjacent teeth carry a compensating increase in load to maintain torque equilibrium. The magnitude of load increase on Teeth 28 and 2 closely matches the load reduction observed on Tooth 1 across all pit depths and friction conditions.

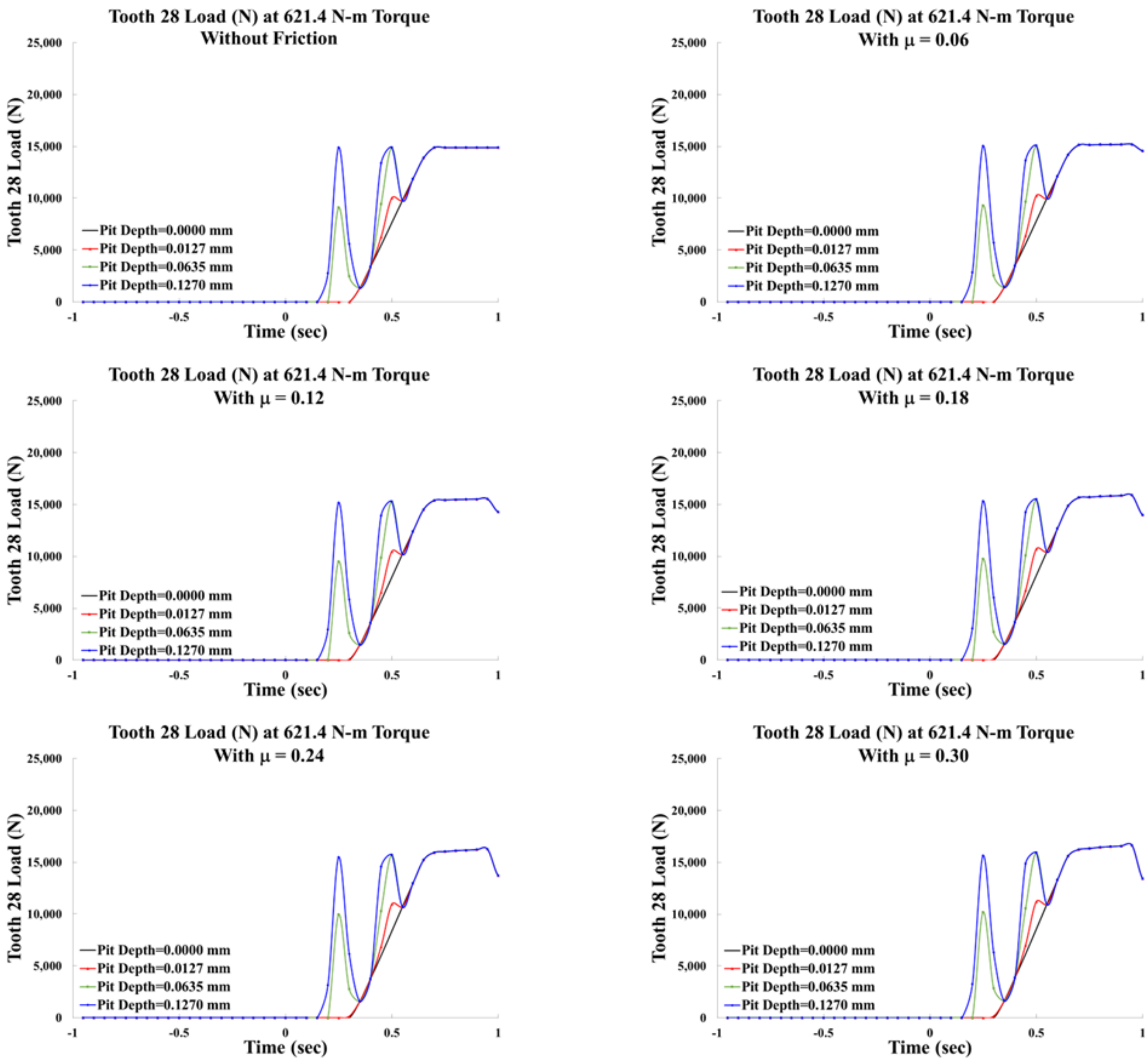

Fig. 8. Tooth number 28 load variations at different pits and friction.

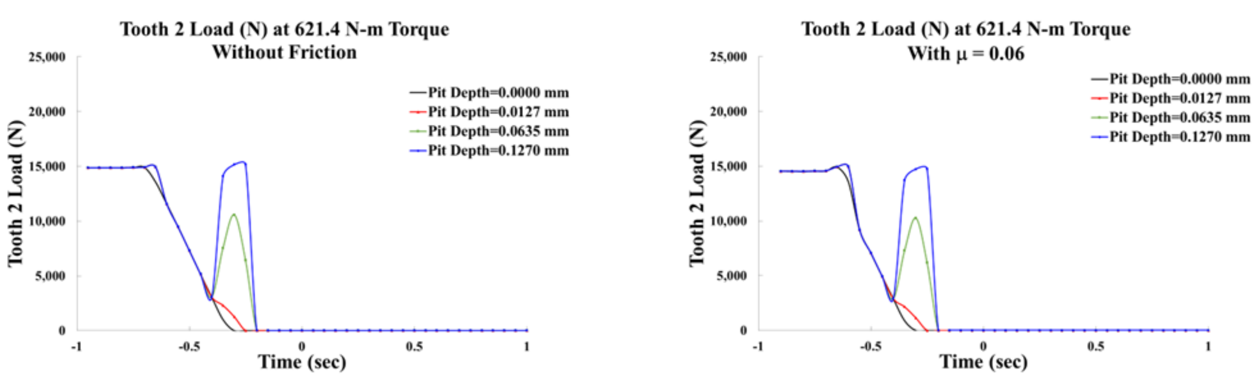

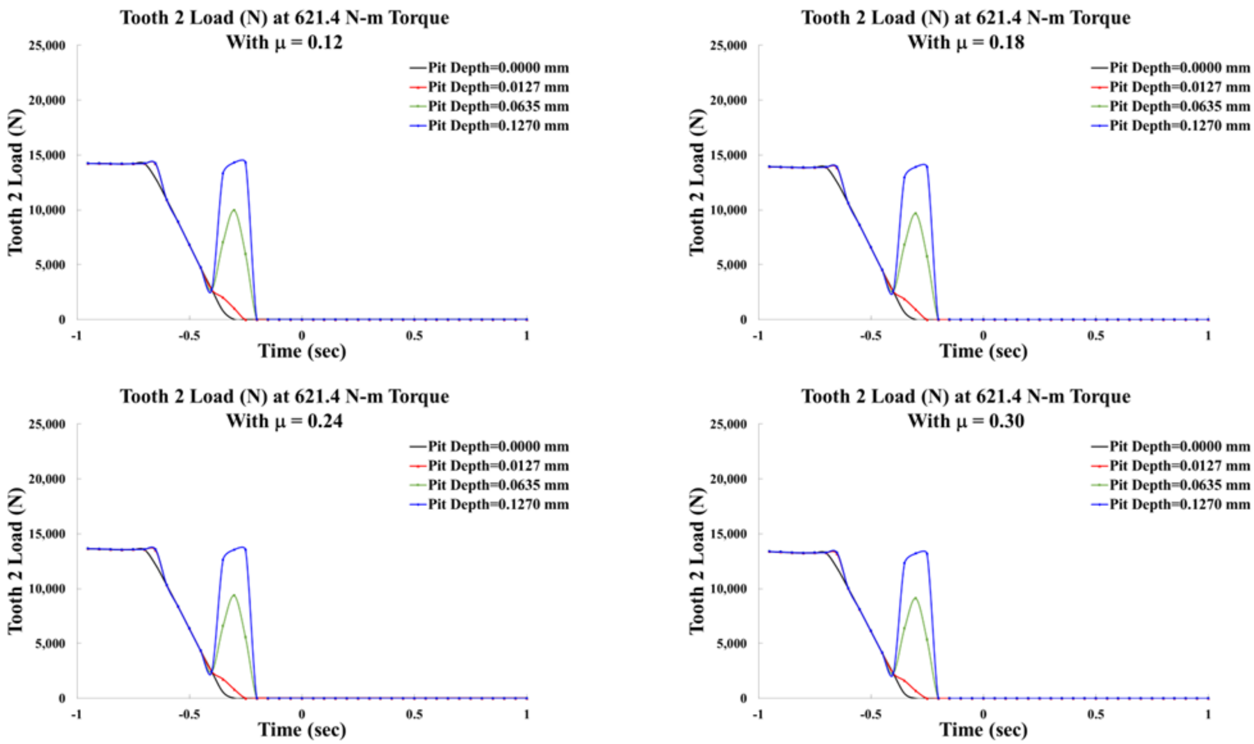

Fig. 9. Tooth number 2 load variations at different pits and friction.

E. Stress Response

The variation of Von Mises root stress for different pit locations and friction coefficients is presented in Fig. 10. For the undamaged case, root stress increases with increasing friction, and the stress variation becomes less smooth as friction increases.

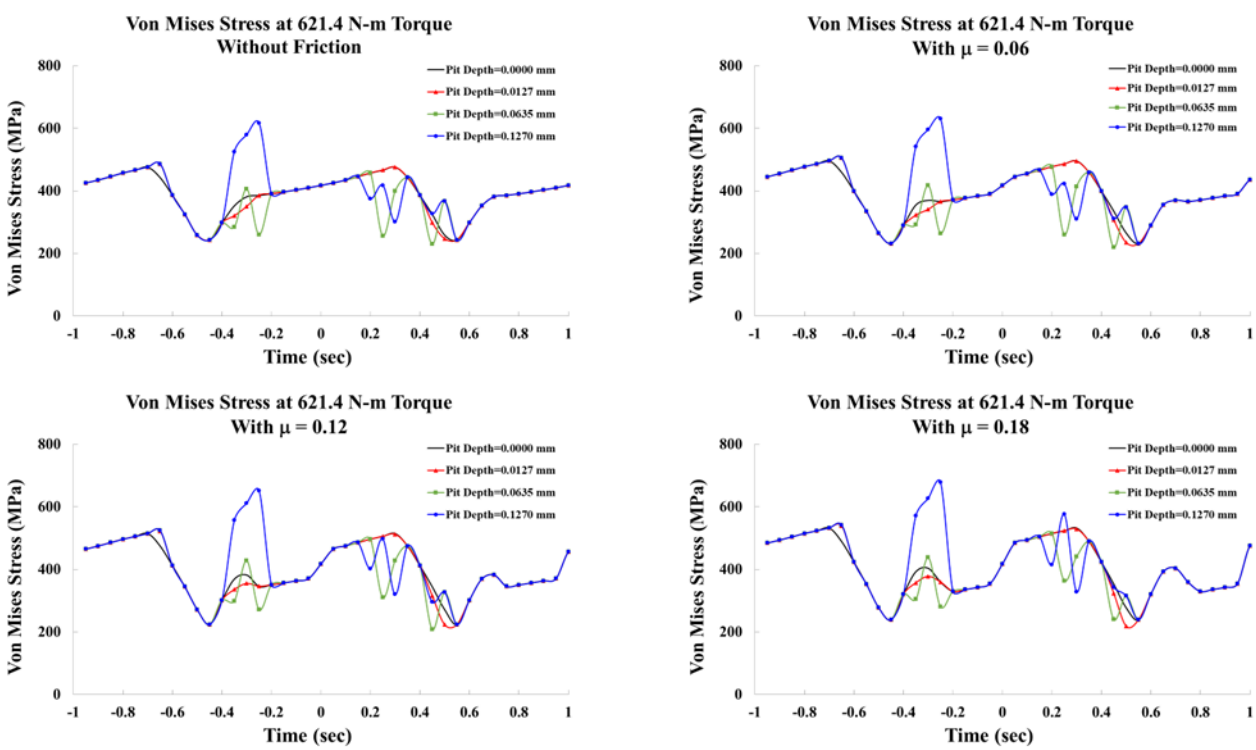

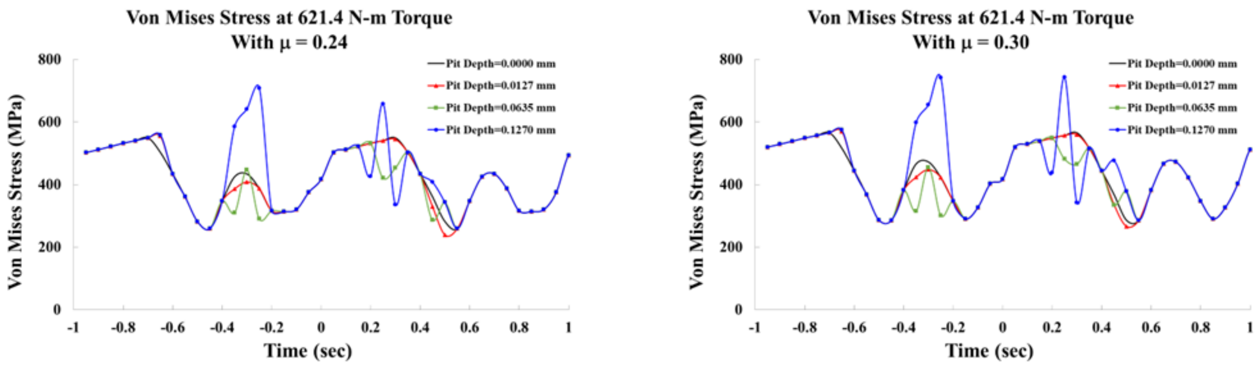

Fig. 10. Von Mises stress variations at different pits and friction.

Pits located adjacent to the pitch point generate significantly higher root stress compared to pits located farther away. The pit adjacent to the pitch point on the dedendum side exhibits the highest root stress and the largest stress variation. Increasing pit depth and coefficient of friction generally leads to increased root stress variation for all pit locations except the pit located exactly at the pitch point.

The maximum Von Mises root stress for all pit locations and friction conditions is compared in Fig. 11. The maximum stress increases monotonically with both pit depth and friction coefficient.

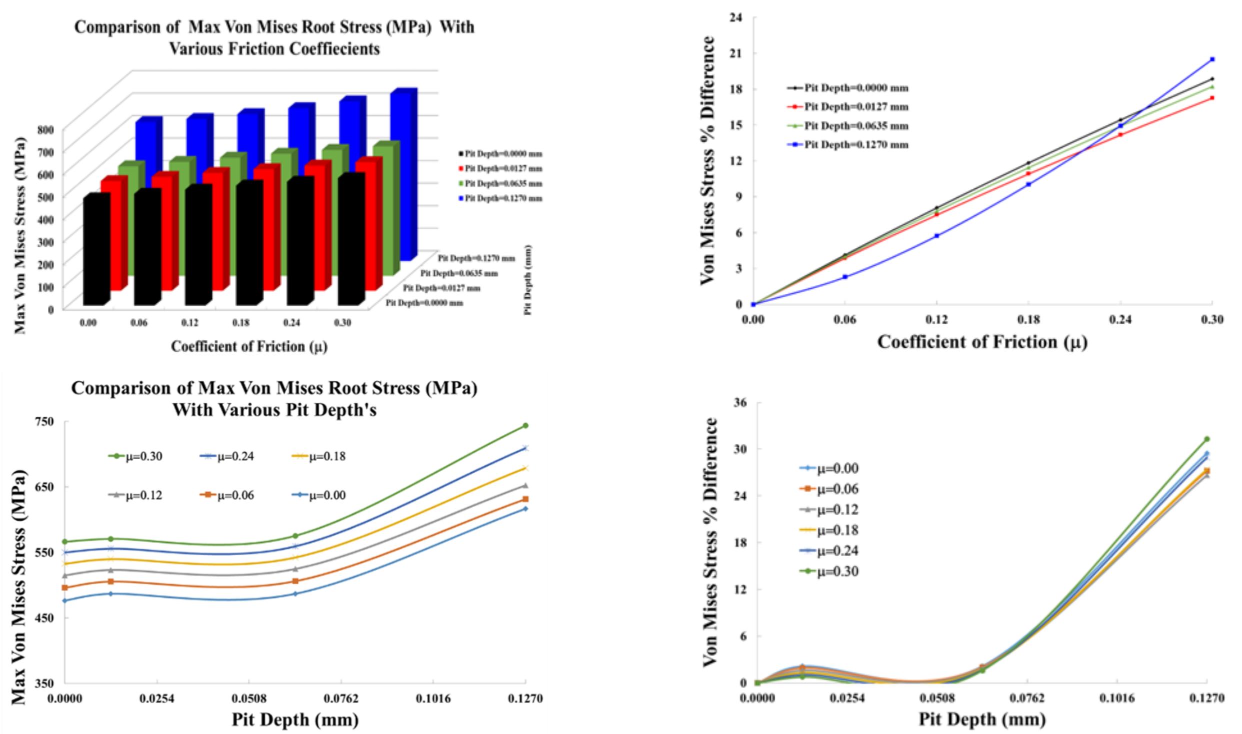

Fig. 11. Comparison of maximum Von Mises root stress at various pits and frictions.

F. *Contact Stress*

Figure 12 shows the variation in contact stress for different pit locations and friction coefficients. Contact stress decreases when the mating tooth engages the pitted region and becomes zero for a portion of the mesh cycle for the maximum pit depth, indicating complete loss of contact. Contact stress increases with increasing coefficient of friction for all pit configurations.

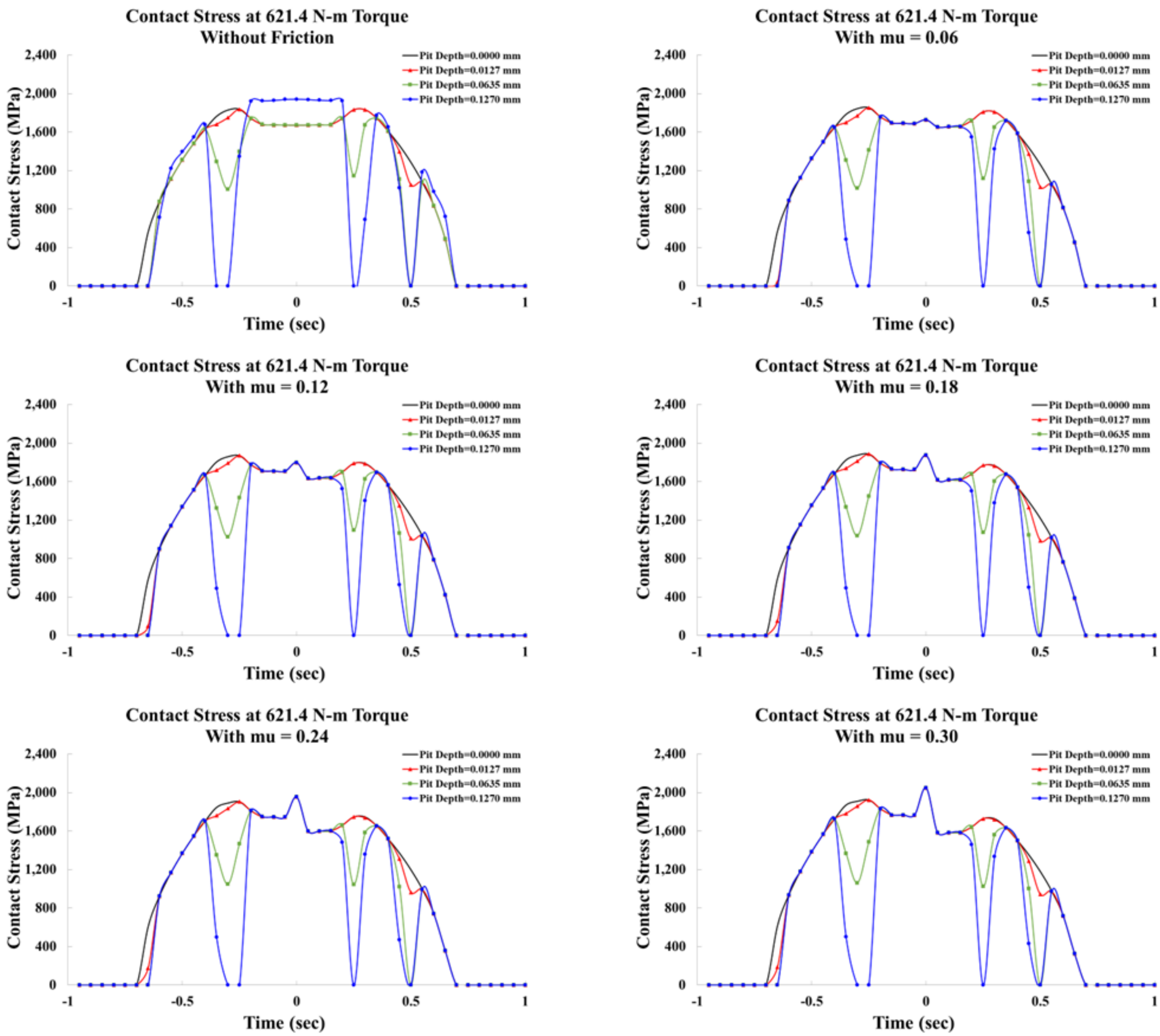

Fig. 12. Comparison of contact stress at various pits and friction magnitudes.

G. Gear Moment and Bearing Forces

The variation in gear moment is shown in Fig. 13. For the undamaged case, gear moment variation increases with increasing friction. Damage located adjacent to the pitch point affects gear moment differently depending on location: variation is reduced for dedendum-side pits and increased for addendum-side pits. Damage at the pitch point has no observable effect on gear moment variation.

The average gear moment is lower than the applied input torque of 621 N·m when damage is present, indicating torque loss due to surface pitting. For a given friction coefficient, increasing pit depth leads to a reduction in average output torque.

Bearing force variation for different pit depths and friction coefficients is shown in Fig. 14. Bearing force variation increases with increasing friction for both damaged and undamaged cases. The presence of pits introduces additional fluctuations at pit engagement locations, with larger pit depths producing greater variation. The pit adjacent to the pitch point on the dedendum side results in the highest bearing force variation.

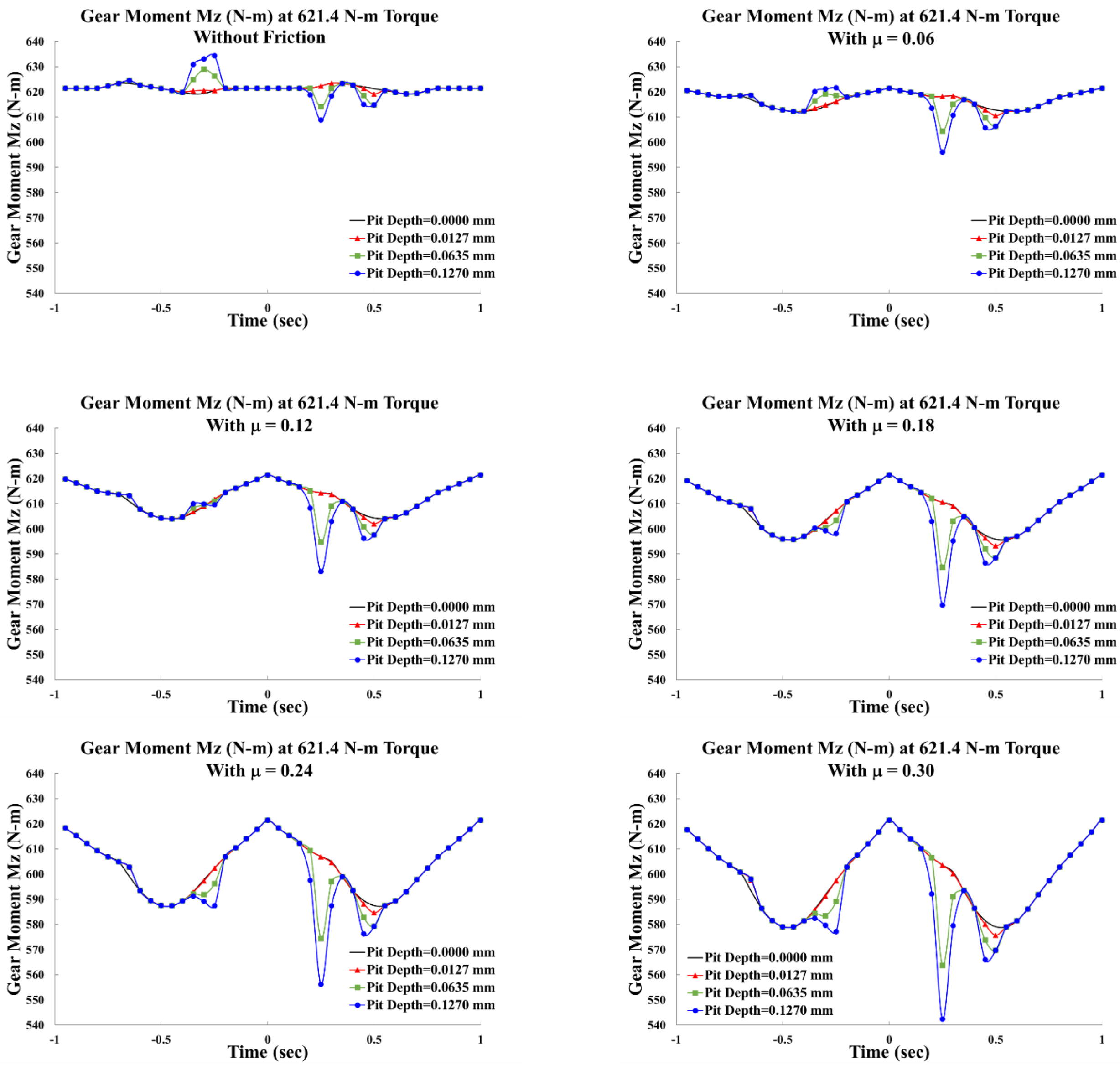

Fig. 13. Comparison of gear moment at various pits and friction coefficients.

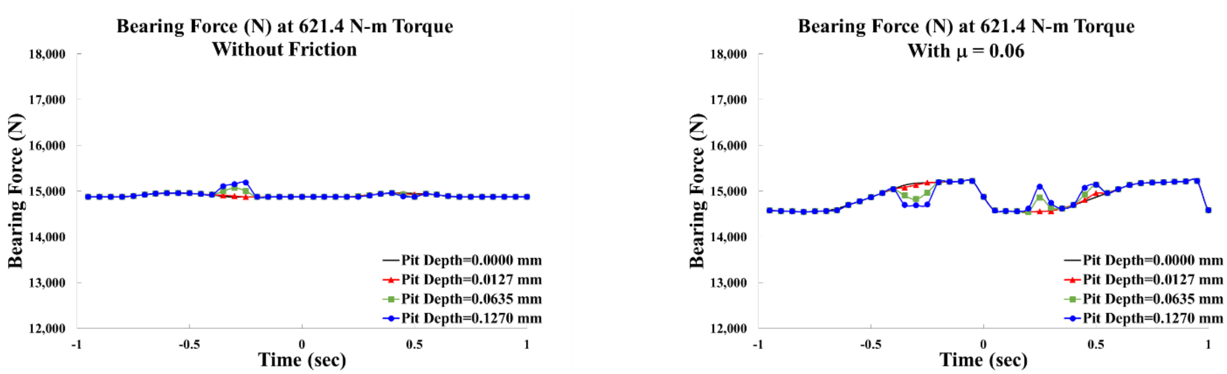

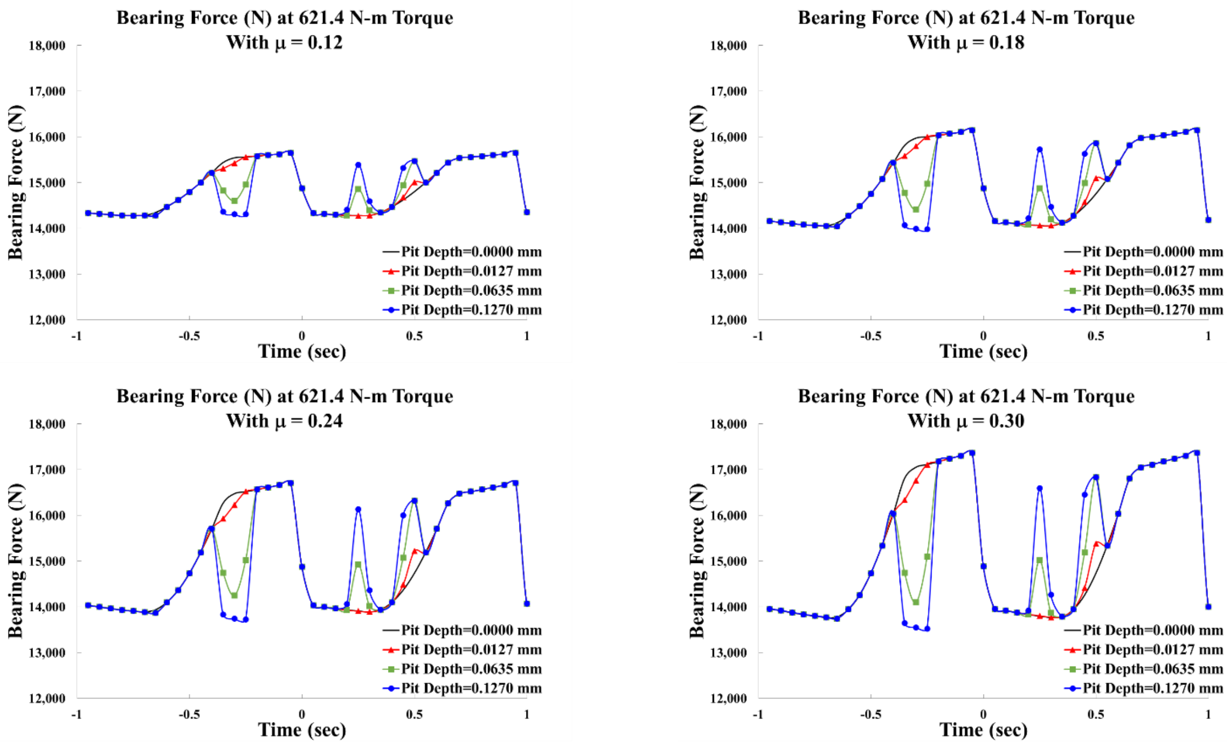

Fig. 14. Comparison of bearing forces at various pits and friction coefficients.

IV. DISCUSSION

The results demonstrate that surface pitting and friction interact strongly to influence gear mesh behavior, with effects extending beyond local contact phenomena to system-level responses.

A. Effect of Pit Location Relative to Pitch Point

Pits located near the pitch point exert the greatest influence on STE, stress, and bearing force variation due to their position within the primary load-carrying region of the mesh. In contrast, pits located far toward the addendum or dedendum extremes have negligible influence because they do not consistently engage the mating tooth. This explains the repeated observation that pitch-point and adjacent pits dominate system response.

B. Friction–Damage Interaction

The interaction between friction and damage exhibits a non-monotonic influence on STE. While friction increases PPTE, the decrease in RMSTE and TATE at higher pit depths suggests that surface damage disrupts sustained elastic excitation, thereby partially masking friction-induced effects. This indicates that severe damage can reduce the sensitivity of certain vibration-related metrics to friction.

C. Load Redistribution Mechanism

Load redistribution among adjacent teeth serves as a primary mechanism for maintaining torque balance when contact is lost due to pitting. This redistribution increases stress on neighboring teeth, which may accelerate fatigue damage outside the initially damaged tooth. Similar mechanisms explain the increase in root stress and bearing force variation observed for deeper pits and higher friction.

D. Noise and Vibration Implications

At the system level, the combined increase in STE, gear moment variation, and bearing force fluctuation indicates elevated potential for vibration and noise. The strong dependence of bearing force variation on both pit depth and friction highlights the importance of including surface damage in gear dynamics assessments, particularly for noise and vibration prediction.

E. Limitations

In this study, quasi-static equations of motion were solved to produce solutions of tooth and bearing force vectors and the resulting gear body motions. The motions were characterized as STE and associated metrics. How such STE manifests to produce noise and vibration and otherwise affect performance will be system dependent. Exploration of gear dynamics in the presence of pits could be accomplished with this model using a dynamic solution. One might also use STE results such as produced herein to guide development of lump parameter gear dynamics models for gears damaged with pits or having other surface anomalies. Such studies would likely be insightful for the purpose of machinery diagnostics and prognostics. However such work is beyond scope of this study.

V. CONCLUSIONS

The following conclusions are drawn from the finite element analysis of spur gears with surface pitting under varying friction conditions.

1. Static transmission error increases with pit depth, as deeper pits cause greater local reductions in mesh stiffness.
2. Pit location strongly influences STE, with damage near the pitch point producing the largest transmission error variations.
3. Increasing the coefficient of friction generally increases STE variation, reflecting strong coupling between frictional forces and elastic tooth deformation.
4. Tooth load decreases locally when the mating tooth engages a pitted region; however, pits located at the pitch point have minimal direct influence on instantaneous tooth load.
5. Load lost due to damage on a given tooth is redistributed to adjacent teeth in order to maintain overall torque equilibrium.
6. At and near the pitch point, tooth load increases with increasing friction coefficient due to enhanced tangential force transmission.
7. Tooth root stress increases as the tooth engages pitted regions, with stress variation becoming more pronounced for deeper pits.
8. Root stress variation increases with friction, indicating that friction amplifies stress fluctuations in damaged teeth.
9. Contact stress decreases within damaged regions and approaches zero for the deepest pits before increasing as contact re-establishes on undamaged surfaces.
10. Gear moment variation increases with pit depth and friction, reflecting increased nonuniformity in load transfer.
11. Bearing force variation increases with both pit depth and friction, demonstrating that surface damage has system-level implications extending beyond the gear mesh.

ACKNOWLEDGMENT

The authors would like to thank NASA Glenn Research Center, Bradley University, and Advanced Numerical Solutions Hilliard, Ohio. Partial support for this work in the form of graduate assistantship was from Dr. Jeffrey Bakken, Dean of Graduate School at Bradley University.

REFERENCES

[1] Bonori, Giorgio, and Francesco Pellicano. "Non-smooth dynamics of spur gears with manufacturing errors." Journal of Sound and Vibration 306, no. 1-2 (2007): 271-283.

[2] Chaari, Fakher, Tahar Fakhfakh, Riadh Hbaieb, Jamel Louati, and Mohamed Haddar. "Influence of manufacturing errors on the dynamic behavior of planetary gears." The International Journal of Advanced Manufacturing Technology 27, no. 7-8 (2006): 738-746.

[3] Hbaieb, R., F. Chaari, T. Fakhfakh, and M. Haddar. "Influence of eccentricity, profile error and tooth pitting on helical planetary gear vibration." Machine Dynamics Problems 29, no. 3 (2005): 5-32.

[4] Randall, R. B. "A new method of modeling gear faults." Journal of Mechanical Design 104, no. 2 (1982): 259-267.

[5] McFadden, P. D. "Examination of a technique for the early detection of failure in gears by signal processing of the time domain average of the meshing vibration." Mechanical systems and signal processing 1, no. 2 (1987): 173-183.

[6] McFadden, P. D. "Determining the location of a fatigue crack in a gear from the phase of the change in the meshing vibration." Mechanical Systems and Signal Processing 2, no. 4 (1988): 403-409.

[7] Zakrajsek, James J., Robert F. Handschuh, David G. Lewicki, and Harry J. Decker. "Detecting gear tooth fracture in a high contact ratio face gear mesh." (1995).

[8] Choy, F. K., V. Polyshchuk, J. J. Zakrajsek, R. F. Handschuh, and D. P. Townsend. "Analysis of the effects of surface pitting and wear on the vibration of a gear transmission system." Tribology international 29, no. 1 (1996): 77-83.

[9] Kuang, J. H., and A. D. Lin. "The effect of tooth wear on the vibration spectrum of a spur gear pair." Journal of Vibration and Acoustics 123, no. 3 (2001): 311-317.

[10] Dempsey, Paula J. "Gear damage detection using oil debris analysis." (2001).

[11] Howard, Ian, Shengxiang Jia, and Jiande Wang. "The dynamic modelling of a spur gear in mesh including friction and a crack." Mechanical systems and signal processing 15, no. 5 (2001): 831-853.

[12] Decker, Harry J. Gear crack detection using tooth analysis. No. ARL-TR-2681. ARMY RESEARCH LAB CLEVELAND OH*, 2002.

[13] Liu, Lin, and Darryll J. Pines. "The influence of gear design parameters on gear tooth damage detection sensitivity." Journal of mechanical design 124, no. 4 (2002): 794-804.

[14] Endo, H., R. B. Randall, and C. Gosselin. "The effects of localized gear tooth damage on the gear dynamics-a comparison of the effect of a gear tooth root crack and a spall on the gear transmission error." In Proceedings I. Mech. E. 8th International Conference on Vibrations in Rotating Machinery, Swansea, UK, pp. 333-342. 2004.

[15] Chaari, F., T. Fakhfakh, and M. Haddar. "Dynamic analysis of a planetary gear failure caused by tooth pitting and cracking." Journal of Failure Analysis and Prevention 6, no. 2 (2006): 73-78.

[16] Hbaieb, R., F. Chaari, T. Fakhfakh, and M. Haddar. "Influence of eccentricity, profile error and tooth pitting on helical planetary gear vibration." Machine Dynamics Problems 29, no. 3 (2005): 5-32.

[17] Thunuguntla, S., Hood, A., and Cooley, C., *Tooth Mesh Characterization of Spur Gear Pairs with Surface Pitting Damage*, SAE Technical Paper 2023-01-0458, 2023.

[18] Shareef, I., Krantz, T. L., and Abdul, W. A. M., "Influence of Surface Pitting and Friction Coefficient on the Static Transmission Error in Spur Gears," *Int. J. Mech. Eng. Robot. Res.*, Vol. 9, No. 3, 2020.

[19] Happi, K. H. Y., "Experimental Study and Comparative Analysis of Pitting Fault in Spur Gear System," *Journal of Vibroengineering*, 2023.

[20] Czakó, A., Řehák, K., Prokop, A., and Ranjan, V., "Determination of Static Transmission Error of Helical Gears Using Finite Element Analysis," *Journal of Measurements in Engineering*, 2020.

[21] Liu, H., Liu, H., Zhu, C., and Zhou, Y., "A Review on Micropitting Studies of Steel Gears," *Coatings*, Vol. 9, No. 1, 2019.

[22] Im, Dongu, Woo-Jin Chung, Hyunggon Lee, You-Jin Lee, Hyunjoon Sung, Minwook Lee, and Young-Jun Park. "Analysis of gear transmission error in helical gear using enhanced tooth contact analysis model considering measured tooth profile errors." *Scientific Reports* 15, no. 1 (2025): 5981.

[23] Abruzzo, Michele, Marco Beghini, Luca Romoli, and Ciro Santus. "Design for manufacturing of a spur gears profile modification based on the static transmission error for improving the dynamic behavior." *The International Journal of Advanced Manufacturing Technology* 129, no. 5 (2023): 1999-2010.

[24] Mark, William D., Aaron C. Isaacson, and Matthew E. Wagner. "Transmission-error frequency-domain-behavior of failing gears." *Mechanical Systems and Signal Processing* 115 (2019): 102-119..

[25] Ouyang, Tiancheng, Geng Wang, Liang Cheng, Jinxiang Wang, and Rui Yang. "Comprehensive diagnosis and analysis of spur gears with pitting-crack coupling faults." *Mechanism and Machine Theory* 176 (2022): 104968.

[26] Zhao, Jiang, Chenbo Ma, Yuyan Zhang, Zhengminqing Li, Xiaofeng Yu, and Wei Sheng. "Effect of tooth surface pitting on dynamic characteristics under mixed lubrication." *Engineering Failure Analysis* 167 (2025): 108961.

[27] Xu, Hang, Chenzhou Wei, Wei Gui, Shufeng Yang, Yuanchun He, Guiping Xie, and Yaoting Wu. "Investigation of the impact of cycloidal gear pin tooth wear on transmission error in precision planetary cycloidal reducers." *International Journal of Metrology and Quality Engineering* 15 (2024): 9.

[28] Ren, Fei, Dexi Wang, Guiqin Shi, and Xiaoling Wu. "Investigation on dynamic characteristics of spur gear transmission system with crack fault." *Machines* 10, no. 8 (2022): 664.

[29] Liang, Xi-Hui, Zhi-Liang Liu, Jun Pan, and Ming Jian Zuo. "Spur gear tooth pitting propagation assessment using model-based analysis." *Chinese Journal of Mechanical Engineering* 30, no. 6 (2017): 1369-1382.

[30] Ji, Chengcheng, Jian Zhang, Jiaxin Jian, Chuanmao Lv, and Zhengminqing Li. "Research on Quasi-Static Transmission Error Measurement of Spur Gears Based on the Acceleration Method." *Machines* 13, no. 10 (2025): 941

[31] Parker, R. G., S. M. Vijayakar, and T. Imajo. "Non-linear dynamic response of a spur gear pair: modelling and experimental comparisons." *Journal of Sound and vibration* 237, no. 3 (2000): 435-455.

[32] Wagaj, Parag, and Ahmet Kahraman. "Impact of tooth profile modifications on the transmission error excitation of helical gear pairs." In Proceedings of ESDA2002: 6th biennial conference on engineering systems design and analysis, pp. 1-11. 2002.

[33] Narayanaswamy, R., and C. D. Glynn. "Vibro-acoustic prediction of low-range planetary gear noise of an automotive transfer case." The Shock and Vibration Digest 38, no. 3 (2006): 240-242.

[34] Tamminana, Venkata Krishna, A. Kahraman, and S. Vijayakar. "A study of the relationship between the dynamic factors and the dynamic transmission error of spur gear pairs." (2007): 75-84.

[35] Singh, Avinash, Ahmet Kahraman, and Haris Ligata. "Internal gear strains and load sharing in planetary transmissions: model and experiments." (2008): 072602.

[36] Prueter, Phillip E., Robert G. Parker, and Frank Cunliffe. "A study of gear root strains in a multi-stage planetary wind turbine gear train using a three dimensional finite element/contact mechanics model and experiments." In International Design Engineering Technical Conferences and Computers and Information in Engineering Conference, vol. 54853, pp. 621-633. 2011.

[37] Ericson, Tristan M., and Robert G. Parker. "Experimental measurement and finite element simulation of elastic-body vibration in planetary gears." Mechanism and Machine Theory 160 (2021): 104264.

Appendix A. Experimental Validation of the Hybrid Numerical Gear Contact Model

This appendix documents the experimental validation of a high-fidelity numerical model for planetary gear contact analysis developed under an Army Small Business Innovation Research (SBIR) program by Advanced Numerical Solutions LLC. The validation compares simulated tooth root stresses against experimental strain gage measurements obtained from a helicopter planetary gearbox test program conducted by collaborative Army and NASA research at NASA Glenn Research Center (GRC).

A.1 Numerical Modeling Approach

The numerical framework employs a hybrid finite element–surface integral formulation for contacting mechanical elements. Global gear body compliance is represented using finite elements, while local near-surface Hertzian deformation is computed using analytical elasticity solutions based on surface integrals. Tooth surface geometry is defined analytically using exact involute representations, rendering contact accuracy independent of finite element mesh density. Compatibility between the analytical inner region and the finite element outer region is enforced at an automatically selected matching interface, ensuring numerical robustness and solution consistency.

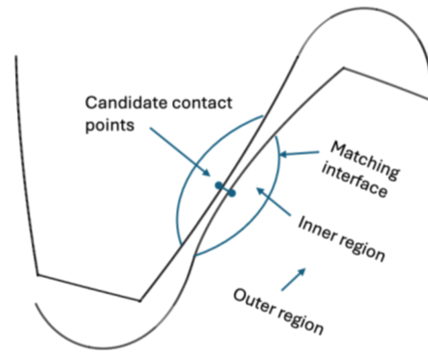

Figure A1: Hybrid finite element–surface integral formulation for gear contact analysis.

A.2 Experimental Test Configuration

Experimental validation data were obtained from a helicopter planetary gearbox test program conducted at NASA GRC. Strain gages were applied to the sun gear and stationary ring gear at the fillet regions on the driving side of selected teeth, corresponding to expected maximum tensile stress locations. Tests were conducted at design torque and maximum rated speed, and strain time histories were recorded under representative operating conditions.

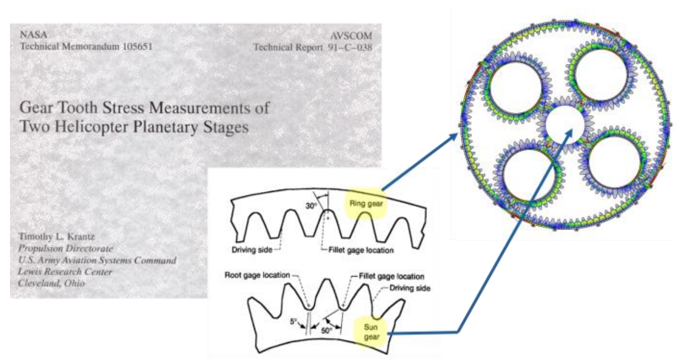

Figure A2: Strain gage locations for sun and ring gears in helicopter planetary gearbox.

A.3 Sun Gear Validation Results

Simulated and experimentally measured sun gear tooth root stresses demonstrate strong agreement in waveform characteristics and stress magnitude. The numerical model reproduces the non-sinusoidal strain response observed experimentally, which results from elastic deformation of the thin-rimmed hollow sun gear. Under load, the sun gear exhibits a multi-lobed deformation pattern that influences local tooth root strain between successive tooth engagements.

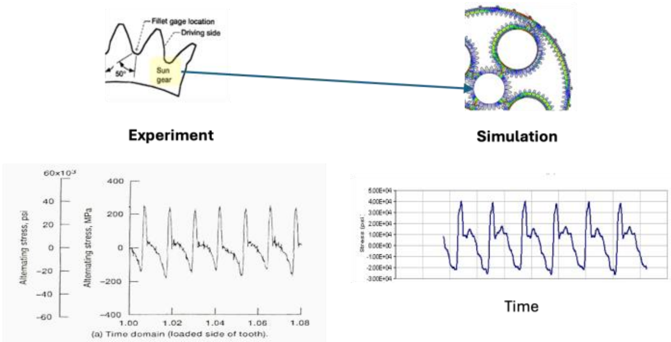

Figure A3: Comparison of measured and simulated sun gear tooth root strain responses.

A.4 Ring Gear Validation Results

Ring gear validation results show close agreement between measured and simulated tooth root stresses. Accurate correlation required modeling of the ring gear spline interface using contact analysis to represent mounting compliance and radial clearance. The ring gear deforms into a four-lobe pattern due to planet gear loading, and this deformation rotates at the planet carrier orbital speed, producing the characteristic curved stress response observed between tooth loading events.

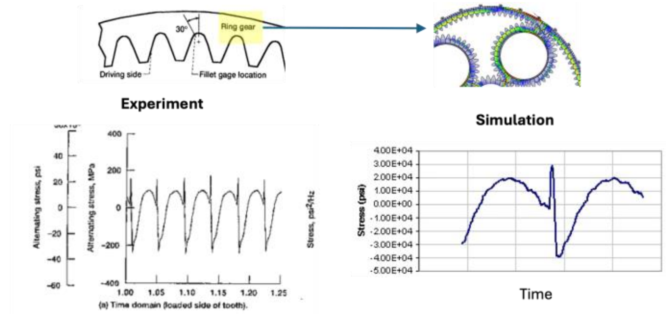

Figure A4: Comparison of measured and simulated ring gear tooth root strain responses.

A.5 Discussion

The agreement between simulation and experiment for both sun and ring gears demonstrates that the hybrid numerical framework accurately captures local contact stresses, global elastic deformation, and load transfer mechanisms in planetary gear systems. The results provide confidence in the predictive capability of the model for high-fidelity gear analysis and durability assessment.